The Meteoritical Society

Meteoritics & Planetary Science 42, Nr 12, 2067–2077 (2007)
Abstract available online at http://meteoritics.org

Mass-dependent fractionation of nickel isotopes in meteoritic metal

David L. COOK[1, 2, 3†*], Meenakshi WADHWA[1, 2, 3††], Robert N. CLAYTON[1, 2, 4], Nicolas DAUPHAS[1, 2, 4], Philip E. JANNEY[3††], and Andrew M. DAVIS[1, 2, 4]

[1]Department of the Geophysical Sciences, The University of Chicago, 5734 South Ellis Avenue, Chicago, Illinois 60637, USA
[2]Chicago Center for Cosmochemistry, 5640 South Ellis Avenue, Chicago, Illinois 60637, USA
[3]Department of Geology, The Field Museum, 1400 South Lake Shore Drive, Chicago, Illinois 60605, USA
[4]Enrico Fermi Institute, 5640 South Ellis Avenue, Chicago, Illinois 60637, USA
[†]Present address: Department of Chemistry and Chemical Biology, Rutgers University, 610 Taylor Road, Piscataway, New Jersey 08854, USA
[††]Present address: Center for Meteorite Studies, School of Earth and Space Exploration, Arizona State University, P.O. Box 871404, Tempe, Arizona 85287–1404, USA
[*]Corresponding author. E-mail: davecook@rci.rutgers.edu

(Received 02 February 2007; revision accepted 08 June 2007)

Abstract–We measured nickel isotopes via multicollector inductively coupled plasma mass spectrometry (MC-ICPMS) in the bulk metal from 36 meteorites, including chondrites, pallasites, and irons (magmatic and non-magmatic). The Ni isotopes in these meteorites are mass fractionated; the fractionation spans an overall range of ≈0.4‰ amu^{-1}. The ranges of Ni isotopic compositions (relative to the SRM 986 Ni isotopic standard) in metal from iron meteorites (≈0.0 to ≈0.3‰ amu^{-1}) and chondrites (≈0.0 to ≈0.2‰ amu^{-1}) are similar, whereas the range in pallasite metal (≈–0.1 to 0.0‰ amu^{-1}) appears distinct. The fractionation of Ni isotopes within a suite of fourteen IIIAB irons (≈0.0 to ≈0.3‰ amu^{-1}) spans the entire range measured in all magmatic irons. However, the degree of Ni isotopic fractionation in these samples does not correlate with their Ni content, suggesting that core crystallization did not fractionate Ni isotopes in a systematic way. We also measured the Ni and Fe isotopes in adjacent kamacite and taenite from the Toluca IAB iron meteorite. Nickel isotopes show clearly resolvable fractionation between these two phases; kamacite is heavier relative to taenite by ≈0.4‰ amu^{-1}. In contrast, the Fe isotopes do not show a resolvable fractionation between kamacite and taenite. The observed isotopic compositions of kamacite and taenite can be understood in terms of kinetic fractionation due to diffusion of Ni during cooling of the Fe-Ni alloy and the development of the Widmanstätten pattern.

INTRODUCTION

Studies of the mass-dependent fractionation of stable isotopes of light elements (e.g., H, C, N, O) have been, and still are, a useful tool for investigating early solar system processes operating in the nebula and on parent bodies. The advent of multi-collector ICPMS has greatly expanded the range of elements now available for such investigations, with the transition metals being of particular interest. Studies of Fe isotopes in meteorites (e.g., Zhu et al. 2001, 2002; Kehm et al. 2003; Poitrasson et al. 2004, 2005; Weyer et al. 2005) as well as of Cu and Zn isotopes (Luck et al. 2005) show that these elements underwent mass-dependent fractionation during processes occurring in the early solar system. These studies have attributed mass-dependent fractionation of transition metals to both low- and high-temperature events that took place in the solar nebula and on meteorite parent bodies. Except for isotopic anomalies found in refractory inclusions from carbonaceous chondrites (e.g., Völkening and Papanastassiou 1989, 1990), the isotopes of Fe and Zn appear to have been fractionated from an originally homogeneous reservoir in the early solar system (Zhu et al. 2001; Kehm et al. 2003; Dauphas et al. 2004; Luck et al. 2005).

Analyses of metallic deep-sea spherules have demonstrated that Ni isotopes can be mass fractionated due to evaporation (Davis and Brownlee 1993; Herzog et al. 1994; Engrand et al. 2005). Furthermore, Ni isotopes in metal from various meteorite groups follow a mass-dependent fractionation trend (Moynier et al. 2004, 2005). Nevertheless, the extent and causes of mass-dependent fractionation of Ni isotopes in natural samples remain largely unexplored. Thus, we have analyzed the Ni isotopic composition of meteoritic

metal from chondrites, pallasites, and iron meteorites with the following goals: 1) to constrain the range of mass-dependent fractionation of Ni isotopes in these objects, 2) to examine the possible effects of fractional crystallization of a liquid Fe-Ni alloy during core formation on the isotopic composition of Ni, and 3) to investigate the fractionation of Ni isotopes between kamacite and taenite in iron meteorites.

ANALYTICAL METHODS

Samples and Sample Preparation

Metal from 36 different meteorites was analyzed. These meteorites included 6 chondrites representing the LL, H, EH, CR, and CBa groups, 3 main group pallasites, the Eagle Station pallasite, and 26 iron meteorites from magmatic (IIAB, IID, IIIAB, IVA, IVB) and non-magmatic (IAB) groups. All metal samples from chondrites, pallasites, non-magmatic irons, and some magmatic irons are those for which non-mass-dependent effects in Ni isotopes were previously investigated (Cook et al. 2006). In addition to these, a suite of fourteen IIIAB irons was also selected to investigate the potential effects of core crystallization on Ni isotopes. For this purpose, we acquired six samples from the Field Museum in Chicago and eight from the Natural History Museum in London. These latter eight samples were originally allocated to E. Mullane for an investigation of Fe isotopes (Mullane et al. 2005). Digested but chemically unprocessed aliquots of these samples were obtained from E. Mullane for this study. Aliquots of these fourteen IIIAB irons were derived from dissolved samples of relatively large pieces (0.3 to 1.4 g) to make sure that they were representative of the bulk metal in these meteorites. For all other iron meteorite samples and for pallasite samples, a small piece of fresh metal was cut using a slow speed saw equipped with a diamond wafering blade. Chondrite samples were crushed, and the metal was separated with a hand magnet. Additional details of the sample preparation techniques are described by Cook et al. (2006).

The Toluca IAB iron meteorite was chosen in order to investigate the isotopic fractionation between kamacite and taenite. A polished and etched thick section of Toluca was examined via scanning electron microscopy (SEM) (JEOL 5800 LV with Oxford Link Isis-300 X-ray microanalysis system, University of Chicago) to identify Ni-poor (kamacite) and Ni-rich (taenite) metal. Elemental X-ray maps covering an area of 2.8 cm^2 were acquired for Fe, Ni, S, and P. Five samples were then collected along a traverse of adjacent Ni-poor and Ni-rich metal regions using a computer-controlled microdrill (MicroMill, New Wave Research) equipped with a tungsten carbide mill bit (Brasseler, scriber H1621.11). The drilled pits were ≈400 μm in diameter and 700 μm in depth. Although care was taken to obtain pure samples of kamacite and taenite from Toluca, it is possible that mixtures of both phases were collected, given the depths of the drilled spots. The potential consequences of such sampling issues are addressed in the discussion of the observed isotopic fractionation between kamacite and taenite.

Sample Digestion and Ni Separation

Details of sample digestion and Ni separation are provided by Cook et al. (2006) and are described only briefly here. Metal samples separated from chondrites and two pallasites (Albin and Molong) that contained visible olivine inclusions were digested in 1 M HCl. The solutions were then centrifuged, and the supernatant was decanted (thus, undigested silicate grains were excluded), evaporated to dryness, and redigested in reverse aqua regia (2:1 conc. HNO_3: conc. HCl). All other samples were digested in reverse aqua regia only. Nickel was separated using a combination of anion and cation exchange chromatography. Depending on whether or not there was significant Ti in our sample solutions, we used either a two-column or three-column protocol for Ni separation. Additionally, the Fe fractions for the microdrilled Toluca samples and the six IIIAB samples from the Field Museum were recovered from the first anion exchange column, as described by Dauphas et al. (2004).

Isotopic Measurements

Nickel isotopic measurements were made on a Micromass IsoProbe MC-ICPMS housed in the Isotope Geochemistry Laboratory of the Field Museum. All five stable Ni isotopes (58, 60, 61, 62, 64) were measured simultaneously, and ^{57}Fe and ^{66}Zn were monitored and used to correct for isobaric interferences on ^{58}Ni from ^{58}Fe and on ^{64}Ni from ^{64}Zn. Samples were corrected for instrumental mass bias using the standard-sample bracketing technique. The NIST SRM 986 reference material was used as the bracketing standard, and all Ni isotope data are reported relative to this standard. Each reported Ni datum represents the mean of a minimum of four (but typically five or more) repeat measurements of the sample bracketed by measurements of SRM 986. Iron isotopes were also measured in the microdrilled samples from Toluca and six of the IIIAB irons (see previous section). Iron isotopes were measured on the same instrument, using IRMM-014 as the bracketing standard. A more detailed discussion of the measurement protocols for Ni and Fe isotopic analyses is provided by Cook et al. (2006) and Dauphas et al. (2004), respectively.

Precision and Accuracy

All Ni isotope ratio data are reported relative to SRM 986 in units of permil (‰) as given by:

$$\delta^{i/j} = [(R_{sample} - R_{standard})/R_{standard}] \times 10^3 \quad (1)$$

where R is the $^{i}Ni/^{58}Ni$ ratio (i = 60, 61, 62, or 64). In most

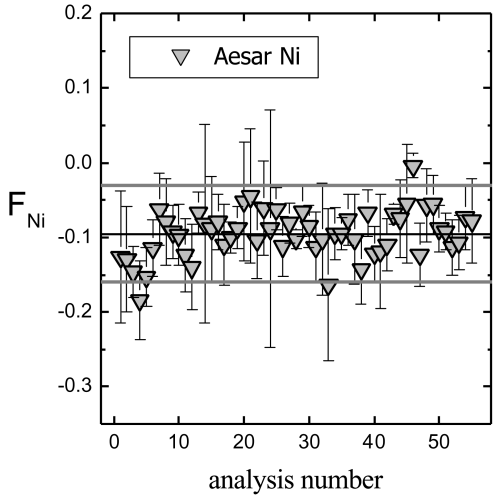

Fig. 1. F_{Ni} values (‰ amu^{-1}) for repeated analyses of an Aesar Ni solution over the course of a 27-month period. Each datum represents the mean of five repeat measurements performed during a single analysis session. The individual error bars (2SE) are based on the five repeat measurements. The external precision is the standard deviation (2SD) based on all of the plotted data and is shown by the two gray lines (±0.065‰ amu^{-1}).

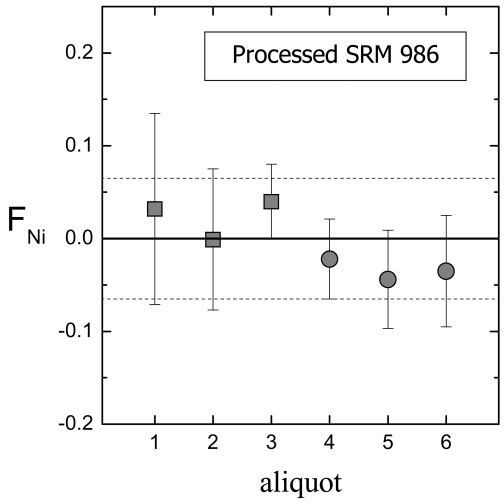

Fig. 2. F_{Ni} values (‰ amu^{-1}) for six aliquots of the SRM 986 isotopic standard processed through our Ni separation procedure (squares: 2-column protocol; circles: 3-column protocol). Plotted errors are 2SE; the external precision (2SD) is shown by the two dashed lines (±0.065‰ amu^{-1}).

cases, the data are discussed using the $^{61}Ni/^{58}Ni$ ratio because this ratio is free from possible effects due to decay of the short-lived isotope ^{60}Fe ($t_{1/2}$ = 1.49 My) and also from potential nucleosynthetic effects on the most neutron-rich Ni isotopes (62 and 64). It is convenient to discuss the mass fractionation effects in terms of permil per amu (‰ amu^{-1}), calculated using:

$$F_{Ni} = \delta^{61/58}/3 \quad (2)$$

The internal precisions of the Ni isotopic compositions of individual samples, based on a number of repeat measurements, are represented by the standard error of the mean (2SE). Repeated analyses of an Aesar Ni solution bracketed with the SRM 986 standard over a 27-month period were used to determine the external precision of our Ni isotope ratio measurements. Figure 1 shows the F_{Ni} values from these measurements; each datum is the mean value calculated from 5 repeat measurements during a single analytical session. These data show that the Aesar Ni solution is mass fractionated relative to SRM 986 by ≈–0.1‰ amu^{-1}, and the external precision (2SD) is ±0.065‰ amu^{-1}. The external precision based on the other Ni isotope ratios is similar ($\delta^{60/58}$/2: ±0.063‰ amu^{-1}; $\delta^{62/58}$/4: ±0.061‰ amu^{-1}; $\delta^{64/58}$/6: ±0.066‰ amu^{-1}).

Isotopic fractionation during chemical processing of samples can potentially affect the isotopic composition and lead to inaccurate measurements. To demonstrate that our Ni separation procedure does not introduce any analytical artifact within uncertainties, three aliquots each of the SRM 986 isotopic standard were processed through both the two-column and the three-column Ni separation protocols (Cook et al. 2006). Figure 2 shows the F_{Ni} values for the six processed aliquots of SRM 986. Within the uncertainties, none of the measured aliquots of the processed SRM 986 have an isotopic composition that differs from the unprocessed SRM 986 used as a bracketing standard. Additionally, no resolvable effects were observed on the other three measured Ni isotope ratios ($\delta^{60/58}$, $\delta^{62/58}$, $\delta^{64/58}$). Hence, these data demonstrate that our Ni separation chemistry does not introduce any resolvable mass-dependent isotopic fractionation effects.

Effects of Fe, Zn, and Signal Intensity

Corrections for isobaric interferences on ^{58}Ni from ^{58}Fe and on ^{64}Ni from ^{64}Zn must be applied if Fe and/or Zn are present in the sample solutions. Furthermore, Fe is the dominant element in meteoritic metal, and an inefficient separation of Ni from Fe could introduce matrix effects that may alter the isotopic measurements. Thus, aliquots of SRM 986 were doped with varying amounts of Fe and Zn (4 aliquots each) to test our ability to correct Fe and Zn interferences and to quantify the possible matrix effects due to the presence of Fe. Figure 3 shows the interference-corrected F_{Ni} values for the SRM 986 aliquots doped with Fe as well as an undoped aliquot. These data show that the Fe interference correction is effective and that no resolvable matrix effects are present for Fe/Ni ≤ 1. Additionally, no resolvable effects were observed on the other three measured Ni isotope ratios ($\delta^{60/58}$, $\delta^{62/58}$, $\delta^{64/58}$) due to the presence of Fe. Cook et al. (2006) showed that the interference correction for ^{64}Zn on ^{64}Ni is not effective for Zn/Ni ≥ 0.01 when measuring non-mass-dependent effects.

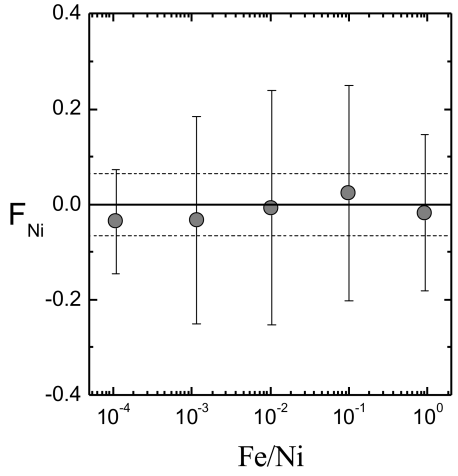

Fig. 3. F_{Ni} values (‰ amu^{-1}) versus the Fe/Ni elemental ratio. Data are from analyses of four aliquots of SRM 986 doped with various concentrations of Fe and one undoped aliquot (Fe/Ni ≈ 10^{-4}). Plotted errors are 2SE; the external precision (2SD) is shown by the two dashed lines (±0.065‰ amu^{-1}).

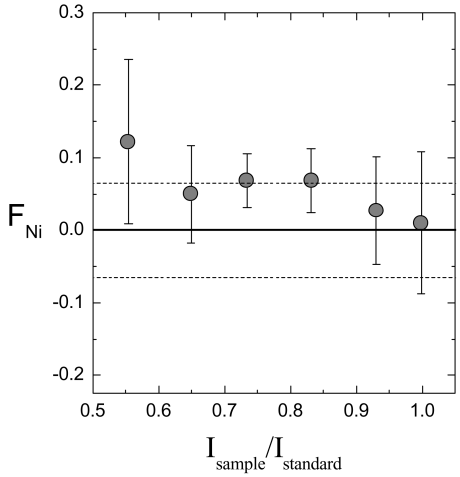

Fig. 4. F_{Ni} values (‰ amu^{-1}) versus the ratio of the sample to standard signal intensity. Data are from analyses of six aliquots of SRM 986 with Ni concentrations ranging from 0.55 to 1.0 ppm bracketed by a 1.0 ppm SRM 986 solution. Plotted errors are 2SE; the external precision (2SD) is shown by the two dashed lines (±0.065‰ amu^{-1}).

This is also true for measurements of mass-dependent effects. However, no resolvable effects were observed on the other three measured Ni isotope ratios ($\delta^{60/58}$, $\delta^{61/58}$, $\delta^{62/58}$) due to the presence of Zn; thus, F_{Ni} was unaffected in the range of Zn/Ni ratios investigated (10^{-5} to 10^{-1}). Similar to our previous work (Cook et al. 2006), all measured sample solutions had Fe/Ni and Zn/Ni ratios $<5.0 \times 10^{-2}$ and $<4.5 \times 10^{-4}$, respectively. The interference correction for F_{Ni} was typically ≤0.01‰ amu^{-1}.

We also investigated whether a mismatch between the Ni signal intensities for standard and sample solutions could affect our mass-dependent isotopic measurements. Six aliquots of SRM 986 with Ni concentrations ranging from 0.55 to 1.0 ppm were analyzed by bracketing with a 1.0 ppm SRM 986 solution. Figure 4 shows the F_{Ni} values from the measurements of these six aliquots of SRM 986. No clearly resolvable effects were observed, except when the sample signal differed from the standard signal by 45%. Similar results were obtained for the other three measured Ni isotope ratios ($\delta^{60/58}$, $\delta^{62/58}$, $\delta^{64/58}$). All measured sample solutions of meteoritic metal had signal intensities within 10% of the standard signal intensity. Thus, all sample and standard signal intensities were matched adequately to provide accurate measurements.

RESULTS AND DISCUSSION

In our previous study of non-mass-dependent effects in Ni isotopes in the metal of chondrites, pallasites, and iron meteorites (Cook et al. 2006), we demonstrated that there are small deficits in the mass-bias-corrected $^{60}Ni/^{58}Ni$ ratio relative to the terrestrial standard (i.e., ε^{60}) in the metal from some primitive chondrites and possibly some iron meteorites, and that these deficits are most likely due to the presence of live ^{60}Fe ($t_{1/2}$ = 1.49 My) at the time of Fe/Ni fractionation in these metal samples. However, there are no other clearly resolvable non-mass-dependent effects in any of the other measured Ni isotope ratios. As such, in Table 1 we present the results of our measurements of the $^{61}Ni/^{58}Ni$, $^{62}Ni/^{58}Ni$, and $^{64}Ni/^{58}Ni$ ratios relative to the SRM 986 standard in permil (i.e., 61/58, 62/58, and 64/58). For each of the samples, the Ni isotope fractionation in terms of permil amu^{-1} is the same within uncertainties regardless of which ratio (i.e., $^{61}Ni/^{58}Ni$, $^{62}Ni/^{58}Ni$, or $^{64}Ni/^{58}Ni$) is considered. Thus, the data are discussed primarily in terms of F_{Ni} (Equation 2).

We note that while we have performed analyses of a single piece of bulk metal from most of the meteorites studied, we analyzed two separate pieces (identified as #1 and #2 in Table 1) of three magmatic IIIAB iron meteorites (Bella Roca, Casas Grandes, and Henbury). Sample #1 in each of these three cases was a small piece (<50 mg) that was previously analyzed primarily to investigate non-mass-dependent effects in Ni isotopes (Cook et al. 2006). We additionally selected a second larger piece (>300 mg) of each of these three samples with the goal of obtaining a representative sample of the bulk metal for our investigation of the mass-dependent fractionation of Ni isotopes in the IIIAB iron meteorites. In the case of Henbury, the Ni isotope compositions of both pieces agree within error. This is not the case for the two pieces of Bella Roca and Casas Grandes. It is likely that the smaller pieces of these two meteorites do not provide representative Ni isotopic compositions of the bulk metal due to the coarseness of the Widmanstätten pattern. Our results for

Table 1. The Ni isotopic composition of meteoritic bulk metal (‰) relative to the SRM 986 standard.

Sample	Group	$\delta^{61/58}$ ± 2SE	$\delta^{62/58}$ ± 2SE	$\delta^{64/58}$ ± 2SE	n
Renazzo[a]	CR	0.47 ± 0.12	0.58 ± 0.10	0.86 ± 0.14	14
Gujba[a]	CBa	0.60 ± 0.12	0.84 ± 0.12	1.21 ± 0.19	13
Semarkona[a]	LL 3.0	0.18 ± 0.12	0.09 ± 0.17	0.16 ± 0.29	10
Bishunpur[a]	LL 3.1	0.43 ± 0.14	0.53 ± 0.18	0.71 ± 0.26	5
Forest Vale[a]	H4	0.53 ± 0.26	0.68 ± 0.20	1.03 ± 0.45	5
Indarch[a]	EH4	0.26 ± 0.21	0.30 ± 0.24	0.49 ± 0.45	5
Eagle Station[a]	PES	0.15 ± 0.05	0.13 ± 0.07	0.39 ± 0.14	5
Albin[a]	PMG	0.02 ± 0.10	0.13 ± 0.09	0.25 ± 0.13	9
Brenham[a]	PMG	–0.25 ± 0.16	–0.34 ± 0.07	–0.34 ± 0.36	5
Molong[a]	PMG	–0.19 ± 0.08	–0.27 ± 0.11	–0.41 ± 0.29	5
Coahuila[a]	IIAB	0.21 ± 0.24	0.32 ± 0.21	0.59 ± 0.61	5
Santa Luzia[a]	IIAB	0.59 ± 0.06	0.76 ± 0.04	1.26 ± 0.13	10
Carbo[a]	IID	0.97 ± 0.41	1.30 ± 0.45	1.90 ± 0.86	5
Augustinovka[b]	IIIAB	–0.05 ± 0.22	–0.12 ± 0.27	–0.20 ± 0.61	5
Avoca[b]	IIIAB	0.22 ± 0.17	0.28 ± 0.24	0.35 ± 0.26	5
Bald Eagle[b]	IIIAB	0.36 ± 0.26	0.54 ± 0.18	0.85 ± 0.51	5
Bear Creek	IIIAB	0.15 ± 0.22	0.27 ± 0.23	0.61 ± 0.39	5
Bella Roca #1[a]	IIIAB	0.08 ± 0.16	0.10 ± 0.12	0.05 ± 0.14	8
Bella Roca #2[b]		0.92 ± 0.25	1.17 ± 0.23	1.77 ± 0.45	5
Carthage	IIIAB	0.55 ± 0.06	0.66 ± 0.07	1.08 ± 0.10	5
Casas Grandes #1[a]	IIIAB	0.62 ± 0.03	0.82 ± 0.03	1.35 ± 0.09	14
Casas Grandes #2		0.29 ± 0.12	0.37 ± 0.04	0.61 ± 0.06	5
Grant	IIIAB	0.13 ± 0.24	0.10 ± 0.20	0.23 ± 0.39	5
Henbury #1[a]	IIIAB	0.33 ± 0.04	0.42 ± 0.04	0.61 ± 0.07	14
Henbury #2[b]		0.31 ± 0.22	0.36 ± 0.16	0.45 ± 0.10	5
Nova Petropolis[b]	IIIAB	0.24 ± 0.13	0.26 ± 0.11	0.30 ± 0.08	5
Orange River Iron[b]	IIIAB	0.23 ± 0.31	0.25 ± 0.41	0.43 ± 0.94	4
Seneca Falls	IIIAB	0.37 ± 0.11	0.50 ± 0.14	0.81 ± 0.15	5
Thunda	IIIAB	0.42 ± 0.16	0.46 ± 0.05	0.73 ± 0.12	5
Welland[b]	IIIAB	0.72 ± 0.58	0.89 ± 0.71	1.40 ± 1.19	5
Gibeon[a]	IVA	0.28 ± 0.21	0.37 ± 0.09	0.78 ± 0.25	5
Yanhuitlan[a]	IVA	0.64 ± 0.18	0.75 ± 0.16	1.12 ± 0.45	5
Cape of Good Hope[a]	IVB	0.36 ± 0.33	0.43 ± 0.14	0.85 ± 0.26	5
Hoba[a]	IVB	0.45 ± 0.11	0.64 ± 0.12	0.94 ± 0.18	13
Tlacotepec[a]	IVB	0.14 ± 0.35	0.22 ± 0.48	0.33 ± 0.69	9
Canyon Diablo[a]	IAB	0.39 ± 0.06	0.51 ± 0.05	0.95 ± 0.12	19
Toluca[a]	IAB	0.44 ± 0.13	0.62 ± 0.09	0.94 ± 0.10	5
Dayton[a]	IAB	–0.15 ± 0.10	–0.14 ± 0.05	0.01 ± 0.35	5
Mundrabilla[a]	IAB	0.26 ± 0.07	0.36 ± 0.06	0.55 ± 0.11	14

[a]Samples previously investigated for non-mass-dependent effects in Ni isotopes (Cook et al. 2006).
[b]Sample solutions provided by E. Mullane.
n = Number of repeat measurements.

individual kamacite and taenite in Toluca (discussed below) show that Ni isotopes are fractionated between these two phases and can lead to mass-dependent Ni isotopic variations in iron meteorites at the millimeter scale. Therefore, small metal samples of iron meteorites (and pallasites) characterized by a coarse Widmanstätten pattern may be skewed toward the isotopic composition of kamacite or taenite. As such, in the discussion on the Ni isotope fractionation in bulk samples of IIIAB iron meteorites, only the larger pieces (samples #2 in Table 1) of each of these three meteorites are considered.

Meteoritic Metal: Bulk Samples

The Ni isotopic compositions of the bulk metal from the 36 meteorites analyzed (Table 1) are shown in a three-isotope plot (Fig. 5). Within error, all samples in Fig. 5 plot on a 1:1 line, which is consistent with mass-dependent isotopic fractionation. The overall range of fractionation is 0.41‰ amu^{-1}. The observed mass-dependent fractionation and the overall range are both consistent with the results previously reported by Moynier et al. (2004, 2005) for metal from iron meteorites, pallasites, chondrites, and mesosiderites.

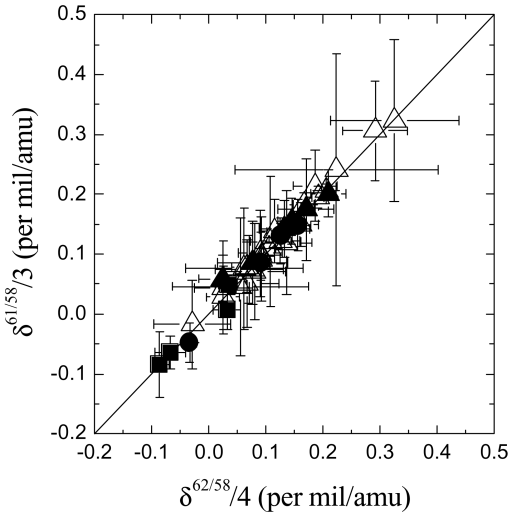

Fig. 5. A three-isotope plot of the data from the analyses of bulk metal from 36 meteorites. The data follow the trend expected for mass-dependent fractionation; a line with a slope equal to 1 is shown for reference. The overall range of fractionation is 0.41‰ amu^{-1}. Plotted errors are 2SE. Filled triangles = chondrites; squares = pallasites; open triangles = magmatic irons; circles = non-magmatic irons.

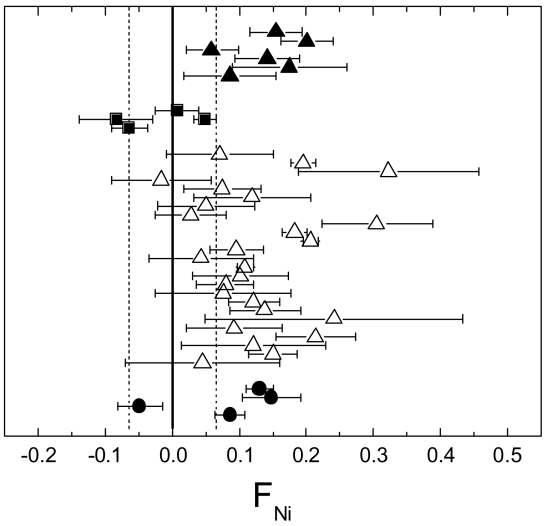

Fig. 6. F_{Ni} values (‰ amu^{-1}) for the bulk metal from 36 meteorites. Plotted errors are 2SE; the external precision (2SD) is shown by the two dashed lines (±0.065‰ amu^{-1}). Filled triangles = chondrites; squares = pallasites; open triangles = magmatic irons; circles = non-magmatic irons.

The F_{Ni} values for all 36 bulk metal samples are plotted in Fig. 6 according to meteorite class. Figure 6 shows that 1) the metal from chondrites and from iron meteorites (magmatic and non-magmatic) is typically similar to or heavier than SRM 986, and 2) metal from pallasites is similar to or lighter than SRM 986. The mean and two standard deviations (2SD) of the F_{Ni} values for each class are as follows: chondrites (0.14 ± 0.11‰ amu^{-1}), iron meteorites (0.12 ± 0.17‰ amu^{-1}), and pallasites (–0.02 ± 0.12‰ amu^{-1}). The Ni isotopic compositions for each meteorite class were compared to one another using t-tests. These comparisons show that there is no significant difference between the chondrites and the iron meteorites (t = 0.417). However, the Ni isotopic composition for pallasite metal is significantly different from both chondrite metal (t = 4.325) and from iron meteorites (t = 3.200). It is possible that the mean Ni isotopic composition of pallasitic metal is biased due to the small number of samples measured. However, if this is not the case, there are several possibilities for explaining the apparently distinct Ni isotopic composition of pallasite metal. If pallasites form at the core-mantle boundary of planetesimals (e.g., Scott 1977), the Ni isotopic composition of pallasite metal may reflect isotopic fractionation between the metallic core and the overlying mantle silicates. Zhu et al. (2002) and Poitrasson et al. (2005) reported that Fe isotopes are fractionated between metal and olivine in pallasites, and these effects range from 0.02 to 0.11‰ amu^{-1}. Recent experiments indicate that Fe isotopes can undergo fractionation up to ≈2.3‰ amu^{-1} between metallic and silicate melts due to kinetic effects (Roskosz et al. 2006) and are fractionated by ≈0.17‰ amu^{-1} between sulfide and silicate melts at temperatures between 840 and 1000 °C due to equilibrium effects (Schuessler et al. 2007). Currently, a lack of Ni isotopic data for non-metal phases from pallasites (e.g., silicates and oxides) precludes an assessment of planetary differentiation as a potential explanation for the apparently distinct Ni isotopic composition of pallasite metal. Alternatively, the Ni isotopic compositions of pallasite metal may reflect differences at the parent-body scale that were established prior to accretion rather than reflecting fractionation effects from differentiation and core formation on their parent bodies. Finally, it is also possible that in the case of some of the smaller samples (i.e., <50 mg) from meteorites with metal that is compositionally heterogeneous on the millimeter-scale (e.g., the four pallasites), the measured Ni isotope compositions may not be representative of the bulk metal in these meteorites. Analyses of additional, and larger, samples would help to ascertain if pallasitic metal does indeed have a mean Ni isotopic composition that differs significantly from metal in other meteorite classes.

IIIAB Iron Meteorites

Nickel Isotopes

With over two hundred members, the IIIABs constitute the largest group of magmatic iron meteorites. These meteorites cover a wide compositional range, and the original IIIAB core is likely well-represented by the large number of samples (Chabot and Haack 2006). Mullane et al. (2005) reported that Fe isotopes from a suite of 33 IIIAB irons were mass fractionated over a large range of 0.49‰ amu^{-1}; however, the Fe isotopic compositions did not correlate with

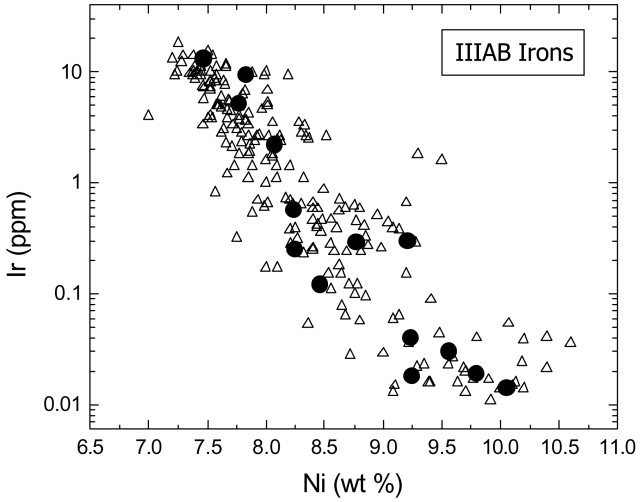

Fig. 7. A plot of Ir versus Ni abundances for members of the IIIAB iron meteorite group. The fourteen samples selected for Ni isotopic analyses are shown by the black circles. Data are from Scott et al. (1973), Scott and Wasson (1976), Kracher et al. (1980), Malvin et al. (1984), and Wasson et al. (1989, 1998).

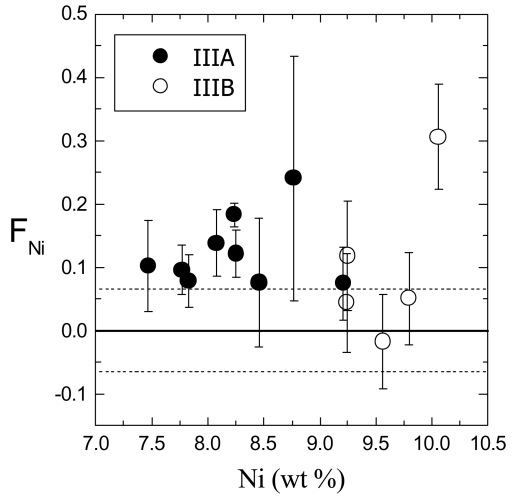

Fig. 8. F_{Ni} values (‰ amu^{-1}) versus Ni abundances for IIIAB irons. Plotted errors are 2SE; the external precision (2SD) is shown by the two dashed lines (±0.065‰ amu^{-1}). Nickel abundance data are from Scott et al. (1973), Scott and Wasson (1976), and Malvin et al. (1984).

the Ni contents, which are a proxy for the degree of crystallization of the metallic core (e.g., Scott 1972). Hence, fourteen IIIAB irons were selected to examine the degree of mass-dependent fractionation of Ni isotopes possibly due to fractional crystallization of the core and to determine whether the fractionation effects on Fe and Ni isotopes were correlated. Figure 7 shows the individual members of the IIIAB group in terms of their Ir and Ni contents, including the fourteen samples chosen for Ni isotopic analyses. Samples were chosen to represent the full compositional range of the IIIAB irons. Figure 8 shows the F_{Ni} values for the fourteen IIIAB irons. The Ni isotopes show fractionation over a considerable range from –0.02 to 0.31‰ amu^{-1}. The earlier crystallized low-Ni IIIA irons and the later crystallized high-Ni IIIB irons have similar mean compositions of 0.1‰ amu^{-1}. Furthermore, the degree of mass fractionation of Ni isotopes does not correlate with the Ni content (r^2 = 0.003). The data in Fig. 8 suggest that core crystallization did not mass fractionate Ni isotopes in a systematic way.

The isotopic composition of Ni in different IIIAB iron meteorites likely reflects a combination of events such as fractionation between 1) liquid metal and silicate during core segregation, 2) immiscible melts in the molten core, and 3) various phases during core solidification. The later stages of core crystallization of iron meteorites were likely affected by liquid immiscibility, resulting in the formation of compositionally distinct liquids due to the presence of S and P in the molten core (Ulff-Møller 1998; Chabot and Drake 2000). Nickel isotopes may have been fractionated as a result of the interaction of a metallic melt with a S and/or P-rich melt during core crystallization. Furthermore, Fe isotopes are fractionated between metal, phosphide (i.e., schreibersite), and sulfide (i.e., troilite) in pallasites (Poitrasson et al. 2005; Weyer et al. 2005) and between metal and sulfide in iron meteorites (Williams et al. 2006). Crystallization followed by slow subsolidus cooling of metallic and non-metallic phases in IIIAB irons may have fractionated Ni isotopes in a similar manner. This last mechanism is particularly appealing because the Ni concentrations are quite different between metal, troilite, and schreibersite in iron meteorites (Buchwald 1977; Jochum et al. 1980). Diffusion of Ni along these concentration gradients during crystallization and cooling of the various phases would likely be accompanied by kinetic isotopic fractionation. The proximity of non-metallic phases relative to the metal could produce metal in iron meteorites with a range of F_{Ni} values and potentially account for the observed variation among the IIIAB irons shown in Fig. 8. Measurements of Ni isotopes in adjacent metallic and non-metallic phases in iron meteorites could be used to test this hypothesis.

Iron Isotopes

Mullane et al. (2005) reported Fe isotope fractionation over a large range (0.49‰ amu^{-1}) for IIIAB irons in which samples were both heavier and lighter than the IRMM-014 standard. These data are inconsistent with other studies of Fe isotopes in IIIAB iron meteorite metal in which all samples had Fe isotopic compositions similar to or slightly heavier than IRMM-014 and spanned a narrow range of 0.07‰ amu^{-1} (Zhu et al. 2001; Kehm et al. 2003; Schoenberg et al. 2006; Williams et al. 2006). We analyzed the Fe isotopes in six of the IIIAB irons with low and high Ni abundances, in which we also measured Ni isotopes. The $^{56}Fe/^{54}Fe$ ratios in ‰ amu^{-1} (or F_{Fe}) for these six samples are

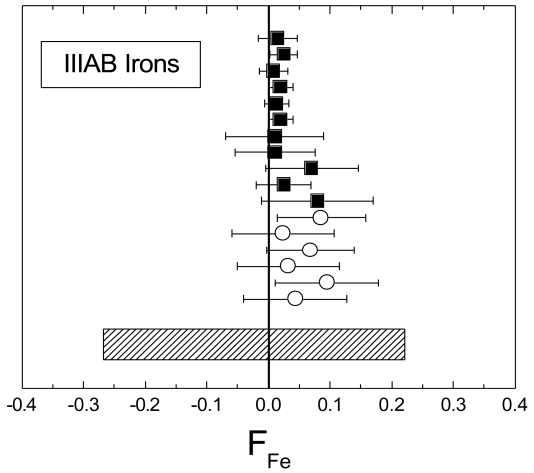

Fig. 9. Fe isotopic compositions (‰ amu^{-1}) for the metal from IIIAB iron meteorites relative to the IRMM-014 standard. $F_{Fe} = \delta^{56/54}/2$. Circles = this study; squares = Zhu et al. 2001; Kehm et al. 2003; Schoenberg et al. 2006; Williams et al. 2006; hatched area = range reported by Mullane et al. (2005).

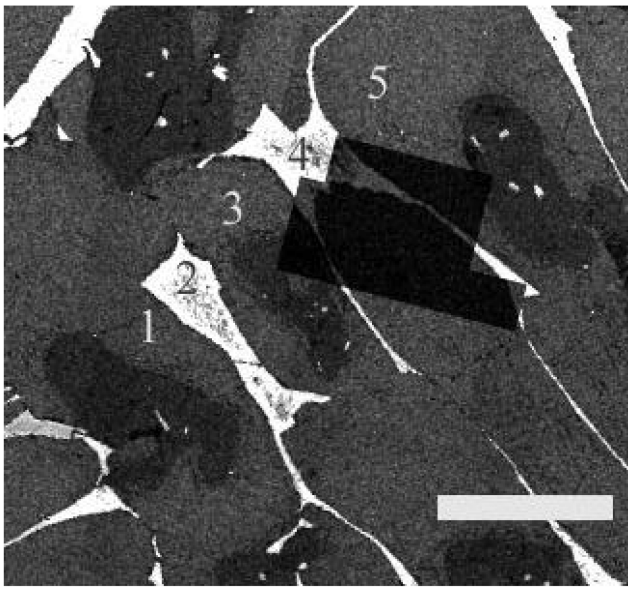

Fig. 10. SEM X-ray Ni map for the region of the Toluca IAB iron chosen for microdrilling. The numbers show the five spots sampled with the microdrill. Bright areas are Ni-rich. Scale bar is 1000 μm.

shown in Fig. 9, along with Fe isotope data for IIIABs from other studies. As shown in Fig. 9, our measurements do not show the large range reported by Mullane et al. (2005). All six samples have Fe isotopic compositions similar to or somewhat heavier than IRMM-014 and span an overall range of only 0.07‰ amu^{-1}. Both of these features are consistent with the measurements of Zhu et al. (2001), Kehm et al. (2003), Schoenberg et al. (2006), and Williams et al. (2006). Furthermore, there is no correlation between the Ni and Fe isotopic compositions of these six samples ($r^2 = 0.105$). Our results suggest that the processes that fractionated the Ni isotopes did not affect the Fe isotopes to the same degree or that Ni and Fe isotopes were fractionated by different processes on the IIIAB parent body.

Isotopic Fractionation Between Kamacite and Taenite

Poitrasson et al. (2005) and Horn et al. (2006) showed that Fe isotopes were fractionated between kamacite and taenite in IAB irons. These authors reported that kamacite (Fe-rich phase) is lighter in terms of its Fe isotopic composition relative to taenite (Ni-rich phase). Because Toluca has been studied for both cooling rates (e.g., Wood 1964; Hopfe and Goldstein 2001) and Fe isotopes, it was selected for an investigation of Fe and Ni isotopic fractionation associated with growth of the Widmanstätten pattern. The region of Toluca chosen for analyses is shown in Fig. 10. Samples were collected along a traverse of adjacent kamacite (spots 1, 3, and 5) and taenite (spots 2 and 4). The Ni isotopic composition of these five samples is shown in Fig. 11 and Table 2. Nickel isotopes show clearly resolvable fractionation between these two phases; kamacite is heavier relative to taenite by 0.36‰ amu^{-1}. Bourdon et al. (2006) reported a similar fractionation of Ni isotopes between kamacite and taenite in iron meteorites. The Fe isotopic compositions of the five samples shown in Fig. 10 were also measured, with the results shown in Fig. 12 and Table 2. Unlike the isotopes of Ni, the Fe isotopes do not show a resolvable fractionation between kamacite and taenite. These results are in contrast to those of Poitrasson et al. (2005) and Horn et al. (2006). As discussed below, the reason for this discrepancy is likely due to differences in sampling.

Dauphas and Rouxel (2006) showed that phase growth in a diffusion-limited regime can create diffusive kinetic isotope fractionation between two phases and control the expression of equilibrium isotope fractionation between the co-existing phases. More recently, Dauphas (2007) developed a numerical simulation to model the formation of the Widmanstätten pattern during cooling of Fe-Ni alloy and to calculate the associated fractionation of Ni and Fe isotopes. During formation of the Widmanstätten pattern, nucleation of kamacite occurs in the solid state and its growth is controlled by diffusion (Wood 1964; Goldstein and Ogilvie 1965). It is likely that kinetic isotopic fractionation will accompany this process because light isotopes diffuse faster than heavy isotopes of the same element (e.g., Richter et al. 2003; Roskosz et al. 2006). The model predicts enrichment of light Ni isotopes in taenite relative to kamacite caused by diffusion during cooling and formation of the Widmanstätten pattern in Fe-Ni alloy. These results are consistent with the measured fractionations shown in Fig. 11.

Model results show that diffusion-driven kinetic isotopic fractionation between two phases depends both on

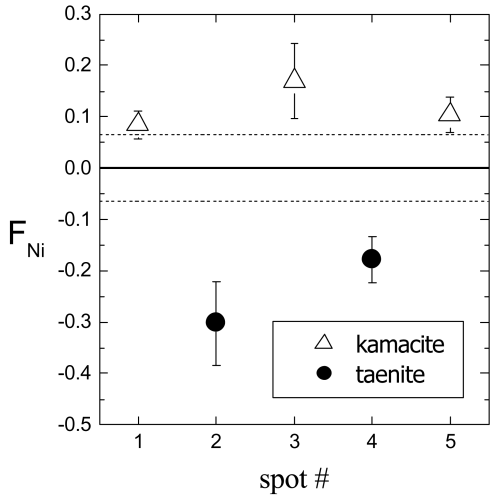

Fig. 11. F_{Ni} values (‰ amu^{-1}) for the five sample spots shown in Fig. 10 for the Toluca IAB iron. Kamacite is heavier relative to taenite by 0.36‰ amu^{-1}. Plotted errors are 2SE; the external precision (2SD) is shown by the two dashed lines (0.065‰ amu^{-1}).

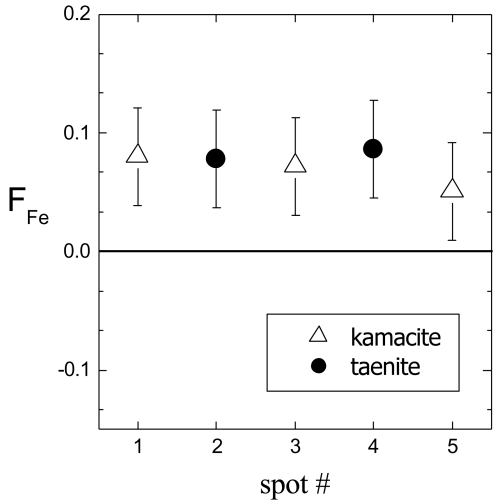

Fig. 12. F_{Fe} values (‰ amu^{-1}) for the five sample spots shown in Fig. 10 for the Toluca IAB iron. Within uncertainty, Fe isotopes show no fractionation between kamacite and taenite.

elemental concentration gradients between the two phases and on the absolute elemental concentrations in each phase. Smaller concentration gradients lead to less fractionation, and large absolute elemental concentrations act to dilute fractionation effects. The absolute Fe concentrations in kamacite and taenite are much greater than the Ni concentrations in these two phases. This factor can account for the difference in the magnitude of the measured fractionations for Ni and Fe isotopes shown in Figs. 11 and 12. Furthermore, inadvertent sampling of kamacite-taenite mixtures in Toluca, by drilling through one phase and into the other, could explain why only resolvable effects in F_{Ni} were measured in this study. Because the Fe/Ni ratios are unequal between kamacite and taenite, the effects on F_{Fe} and F_{Ni} from mixing these two phases during sampling is not linear. Depending on the proportions of kamacite and taenite involved in mixing, F_{Ni} may change rapidly as F_{Fe} changes slowly or vice-versa, relative to the isotopic compositions of the pure phases. For example, mixing taenite and kamacite in a 3:1 ratio changes F_{Fe} by 28%, whereas F_{Ni} changes only by 7.6%, relative to pure taenite. Sampling of pure kamacite and taenite-kamacite mixtures could account for the observed differences in F_{Ni} and lack of observed differences in F_{Fe} between kamacite and taenite in Toluca, as shown in Figs. 11 and 12.

Although the observed isotopic fractionations in Toluca are consistent with kinetic effects (especially given the role of diffusion in formation of the Widmanstätten pattern) equilibrium fractionation cannot be ruled out. Modeling results show that equilibrium and kinetic fractionation effects could potentially be resolved if precise measurements of Ni and Fe isotopes could be made at a higher spatial resolution (i.e., ≈20 μm) than has been achieved thus far.

Table 2. The F_{Ni} and F_{Fe} values (‰ amu^{-1}) for kamacite and taenite from the Toluca IAB iron.

Sample	F_{Ni} ± 2SE	n	F_{Fe} ± 2SE	n
Spot #1 (kamacite)	0.084 ± 0.028	5	0.080 ± 0.041	4
Spot #2 (taenite)	–0.302 ± 0.082	5	0.078 ± 0.041	4
Spot #3 (kamacite)	0.169 ± 0.073	5	0.072 ± 0.041	4
Spot #4 (taenite)	–0.178 ± 0.045	5	0.086 ± 0.041	4
Spot #5 (kamacite)	0.103 ± 0.034	5	0.051 ± 0.041	4

CONCLUSIONS

The Ni isotopes in bulk metal samples from 36 meteorites follow a mass-dependent fractionation trend. These results are consistent with previous work (Moynier et al. 2004, 2005) and imply that Ni isotopes were fractionated from an initially isotopically homogeneous reservoir. The Ni isotopic composition of metal from chondrites and iron meteorites (magmatic and non-magmatic groups) is similar to or heavier than SRM 986, whereas pallasite metal is similar to or lighter than SRM 986. Measurements of additional pallasites are needed to determine whether this difference is real or the result of sampling bias.

A suite of fourteen IIIAB irons shows fractionation over a considerable range. The overall degree of mass fractionation of Ni isotopes does not correlate with the Ni content, suggesting that core crystallization did not mass fractionate Ni isotopes in a systematic way. The variability observed in the IIIAB irons may be due to the interaction of immiscible melts during the later stages of core crystallization or due to the crystallization of metallic and non-metallic phases. Measurements of Ni isotopes in adjacent metal, phosphide, and sulfide phases in iron meteorites are needed to determine the cause of the Ni

isotope variation recorded in the IIIAB irons. Iron isotopes were also measured in six of the IIIAB samples. Within uncertainty, all samples have the same Fe isotopic composition, and we find no evidence of the large range reported by Mullane et al. (2005).

The Ni and Fe isotopes in adjacent kamacite and taenite from the Toluca IAB iron were measured. Nickel isotopes show clearly resolvable fractionation between these two phases; nickel in kamacite is heavier relative to taenite. In contrast, the Fe isotopes do not show a resolvable fractionation between kamacite and taenite. The observed isotopic compositions can be understood in terms of kinetic fractionation due to diffusion during cooling of the Fe-Ni alloy and the development of the Widmanstätten pattern. However, equilibrium fractionation at the interface between kamacite and taenite cannot be ruled out as the cause of the measured isotopic compositions, and future measurements at better spatial resolution could potentially discriminate between equilibrium and kinetic effects.

Acknowledgments–We thank E. Mullane for providing aliquots from her solutions of IIIAB irons, the Smithsonian for providing the sample of Semarkona (USNM 1805), and Greg Herzog and an anonymous reviewer for helpful comments and suggestions. This work was supported in part by the National Aeronautics and Space Administration through grants to M. W., R. N. C., N. D., and A. M. D.

Editorial Handling—Dr. Edward Scott

REFERENCES

Bourdon B., Quitté G., and Halliday A. N. 2006. Kinetic fractionation of nickel and iron between kamacite and taenite: Insights into cooling rates of iron meteorites (abstract). *Meteoritics & Planetary Science* 41:A26.

Buchwald V. F. 1977. The mineralogy of iron meteorites. *Philosophical Transactions of the Royal Society of London A* 286:453–491.

Chabot N. L. and Drake M. J. 2000. Crystallization of magmatic iron meteorites: The effects of phosphorus and liquid immiscibility. *Meteoritics & Planetary Science* 35:807–816.

Chabot N. L. and Haack H. 2006. Evolution of asteroidal cores. In *Meteorites and the early solar system II*, edited by Lauretta D. S. and McSween H. Y. Jr. Tucson, Arizona: The University of Arizona Press. pp. 747–771.

Cook D. L., Wadhwa M., Janney P. E., Dauphas N., Clayton R. N., and Davis A. M. 2006. High-precision measurements of nickel isotopes in metallic samples via multi-collector ICPMS. *Analytical Chemistry* 78:8477–8484.

Dauphas N. 2007. Diffusion-driven kinetic isotope effect of Fe and Ni during formation of Widmanstätten pattern. *Meteoritics & Planetary Science* 42:1597–1613.

Dauphas N., Janney P. E., Mendybaev R. A., Wadhwa M., Richter F. M., Davis A. M., Hines R., and Foley C. N. 2004. Chromatographic separation and multicollection-ICPMS analysis of iron. Investigating mass-dependent and -independent isotope effects. *Analytical Chemistry* 76:5855–5863.

Dauphas N. and Rouxel O. 2006. Mass spectrometry and natural variations of iron isotopes. *Mass Spectrometry Reviews* 25:515–550.

Davis A. M. and Brownlee D. E. 1993. Iron and nickel isotopic mass fractionation in deep-sea spherules (abstract). 24th Lunar and Planetary Science Conference. pp. 373–374.

Engrand C., McKeegan K. D., Leshin L. A., Herzog G. F., Schnabel C., Nyquist L. E., and Brownlee D. E. 2005. Isotopic compositions of oxygen, iron, chromium, and nickel in cosmic spherules: Toward a better comprehension of atmospheric entry heating effects. *Geochimica et Cosmochimica Acta* 69:5365–5385.

Goldstein J. I. and Ogilvie R. E. 1965. The growth of the Widmanstätten pattern in metallic meteorites. *Geochimica et Cosmochimica Acta* 29:893–920.

Herzog G. F., Hall G. S., and Brownlee D. E. 1994. Mass fractionation of nickel isotopes in metallic spheres. *Geochimica et Cosmochimica Acta* 58:5319–5323.

Hopfe W. D. and Goldstein J. I. 2001. The metallographic cooling rate method revised: Application to iron meteorites and mesosiderites. *Meteoritics & Planetary Science* 36:135–154.

Horn I., Blanckenburg F. von, Schoenberg R., Steinhoefel G., and Markl G. 2006. In situ iron isotope ratio determination using UV-femtosecond laser ablation with application to hydrothermal ore formation processes. *Geochimica et Cosmochimica Acta* 70: 3677–3688.

Jochum K. P., Seufert M., and Begemann F. 1980. On the distribution of major and trace elements between metal and phosphide phases of some iron meteorites. *Zeitschrift für Naturforschung* 35a:57–63.

Kehm K., Hauri E. H., Alexander C. M. O'D., and Carlson R. W. 2003. High-precision iron isotope measurements of meteoritic material by cold plasma ICP-MS. *Geochimica et Cosmochimica Acta* 67:2879–2891.

Kracher A., Willis J., and Wasson J. T. 1980. Chemical classification of iron meteorites—IX. A new group (IIF), revision of IAB and IIICD, and data on 57 additional irons. *Geochimica et Cosmochimica Acta* 44:773–787.

Malvin D. J., Wang D., and Wasson J. T. 1984. Chemical classification of iron meteorites—X. Multielement studies of 43 irons, resolution of group IIIE from IIIAB, and evaluation of Cu as a taxonomic parameter. *Geochimica et Cosmochimica Acta* 48:785–804.

Moynier F., Télouk P., Blichert-Toft J., and Albarède F. 2004. The isotope geochemistry of nickel in chondrites and iron meteorites (abstract #1286). 35th Lunar and Planetary Science Conference. CD-ROM.

Moynier F., Blichert-Toft J., Télouk P., and Albarède F. 2005. Excesses of ^{60}Ni in chondrites and iron meteorites (abstract #1593). 36th Lunar and Planetary Science Conference CD-ROM.

Mullane E., Russell S. S., and Gounelle M. 2005. Fractionation of iron isotopes during magmatic processing on the IIIAB parent body (abstract). *Meteoritics & Planetary Science* 40:A108.

Poitrasson F., Halliday A. N., Lee D.-C., Levasseur S., and Teutsch N. 2004. Iron isotope differences between Earth, Moon, Mars, and Vesta as possible records of contrasted accretion mechanisms. *Earth and Planetary Science Letters* 223:253–266.

Poitrasson F., Levasseur S., and Teutsch N. 2005. Significance of iron isotope mineral fractionation in pallasites and iron meteorites for the core-mantle differentiation of terrestrial planets. *Earth and Planetary Science Letters* 234:151–164.

Richter F. M., Davis A. M., DePaolo D. J., and Watson B. E. 2003. Isotope fractionation by chemical diffusion between molten basalt and rhyolite. *Geochimica et Cosmochimica Acta* 67:3905–3923.

Roskosz M., Luais B., Watson H. C., Toplis M. J., Alexander C. M. O' D., and Mysen B. O. 2006. Experimental quantification of the fractionation of Fe isotopes during metal segregation from a silicate melt. *Earth and Planetary Science Letters* 248:851–867.

Schoenberg R. and Blanckenburg F. von. 2006. Modes of planetary-scale Fe isotope fractionation. *Earth and Planetary Science Letters* 252:342–359.

Schuessler J. A., Schoenberg R., Behrens H., and Blanckenburg F. von. 2007. The experimental calibration of the iron isotope fractionation factor between pyrrhotite and peralkaline rhyolitic melt. *Geochimica et Cosmochimica Acta* 71:417–433.

Scott E. R. D. and Wasson J. T. 1976. Chemical classification of iron meteorites—VIII. Groups IC, IIE, IIIF, and 97 other irons. *Geochimica et Cosmochimica Acta* 40:103–115.

Scott E. R. D., Wasson J. T., and Buchwald V. F. 1973. Chemical classification of iron meteorites—VII. A re-investigation of irons with Ge concentrations between 25 and 80 ppm. *Geochimica et Cosmochimica Acta* 37:1957–1983.

Ulff-Møller F. 1998. Effects of liquid immiscibility on trace element fractionation in magmatic iron meteorites: A case study of group IIIAB. *Meteoritics & Planetary Science* 33:207–220.

Völkening J. and Papanastassiou D. A. 1989. Iron isotope anomaly. *The Astrophysical Journal* 347:L43–L46.

Völkening J. and Papanastassiou D. A. 1990. Zinc isotope anomaly. *The Astrophysical Journal* 358:L29–L32.

Wasson J. T., Xinwei O., Wang J., and Jerde E. 1989. Chemical classification of iron meteorites: XI. Multi-element studies of 38 new irons and the high abundance of ungrouped irons from Antarctica. *Geochimica et Cosmochimica Acta* 53:735–744.

Wasson J. T., Choi B.-G., Jerde E. A., and Ulff-Møller F. 1998. Chemical classification of iron meteorites: XII. New members of the magmatic groups. *Geochimica et Cosmochimica Acta* 62: 715–724.

Weyer S., Anbar A. D., Brey G. P., Münker C., Mezger K., and Woodland A. B. 2005. Iron isotope fractionation during planetary differentiation. *Earth and Planetary Science Letters* 240:151–164.

Williams H. M., Markowski A., Quitté G., Halliday A. N., Teutsch N., and Levasseur S. 2006. Fe isotope fractionation in iron meteorites: New insights into metal-sulphide segregation and planetary accretion. *Earth and Planetary Science Letters* 250: 486–500.

Wood J. A. 1964. The cooling rates and parent planets of several iron meteorites. *Icarus* 3:429–459.

Zhu X. K., Guo Y., O'Nions R. K., Young E. D., and Ash R. D. 2001. Isotopic homogeneity of iron in the early solar nebula. *Nature* 412:311–313.

Zhu X. K., Guo Y., Williams R. J. P., O'Nions R. K., Matthews A., Belshaw N. S., Canters G. W., de Waal E. C., Weser U., Burgess B. K., and Salvato B. 2002. Mass fractionation processes of transition metal isotopes. *Earth and Planetary Science Letters* 200:47–62.